

LA-7523-PR

Progress Report

**Stimulation and Characterization of
Eastern Gas Shales**

January—March 1978

University of California



LOS ALAMOS SCIENTIFIC LABORATORY

Post Office Box 1663 Los Alamos, New Mexico 87545

An Affirmative Action/Equal Opportunity Employer

Previous reports in this series, unclassified, are
LA-7094-PR, LA-7320-PR, and LA-7383-PR.

This work was supported by the US Department
of Energy, Division of Fossil Fuel Extraction,
as part of the Eastern Gas Shales Project.

This report was prepared as an account of work sponsored
by the United States Government. Neither the United States
nor the United States Department of Energy, nor any of their
employees, nor any of their contractors, subcontractors, or
their employees, makes any warranty, express or implied, or
assumes any legal liability or responsibility for the accuracy,
completeness, or usefulness of any information, apparatus,
product, or process disclosed, or represents that its use would
not infringe privately owned rights.

UNITED STATES
DEPARTMENT OF ENERGY
CONTRACT W-7405-ENG. 36

LA-7523-PR
Progress Report
Special Distribution
Issued: December 1978

**Stimulation and Characterization of
Eastern Gas Shales
January—March 1978**

Compiled by
G. L. Schott

W. J. Carter and N. E. Vanderborgh
Program Managers



CONTENTS

ABSTRACT	1
I. SUMMARY AND APPRAISAL (G. L. Schott)	1
A. Penetration by Shaped-Charge Jets	1
B. Dynamics of Shale Compression	2
C. Characterization by Laser Pyrolysis	2
II. PENETRATION OF ROCK AND FERROPHOSPHORUS GROUT BY COPPER-CONE JETS (S. P. Marsh)	2
III. DYNAMIC RESPONSE OF SHALE TO HIGH PRESSURE (J. D. Jacobson)	6
IV. PULSED-LASER PYROLYSIS (N. E. Vanderborgh and J. P. Bertino)	12
A. General Approach	12
B. Sample Preparation	14
C. Chromatography	15
D. Tool Design	19
REFERENCES	20
DISTRIBUTION	21

STIMULATION AND CHARACTERIZATION OF EASTERN GAS SHALES

JANUARY—MARCH 1978

Compiled by G. L. Schott

W. J. Carter and N. E. Vanderborgh, Program Managers

ABSTRACT

This report presents the progress of investigations on the use of metal-lined shaped charges for the explosive stimulation of natural gas wells in Devonian shales, and the use of rapid analysis by laser-pyrolysis/gas-chromatography to determine geochemical characteristics of these shales.

Results are presented of small-scale tests that measure the penetration of several shales and grouts by a standard commercial shaped charge. A grout composition of Portland cement with ferrophosphorus sand has been found that simulates the penetrability of shale satisfactorily for continued development work on our tapered liner charges of wellbore scale.

Shock wave Hugoniot data observed in planar impact experiments on Devonian shale core specimens have been systematized for future high-pressure penetration dynamics calculations. The theoretical model used includes mechanical unloading hysteresis and high release-wave speed.

Using controlled techniques devised for analyzing homogenized shale powders, we have achieved a preliminary correlation between the absolute yield of acetylene from pulsed-laser pyrolysis and the independently measured total carbon content.

I. SUMMARY AND APPRAISAL (G. L. Schott)

A. Penetration by Shaped-Charge Jets

Recognizing that the synthetic grout we have used as a standard target in our developmental testing of shaped charges is significantly more penetrable than a limestone having nearly the same bulk density, we have extended our small-scale tests (Ref. 1, pp. 7-11) of the penetrability of different mineral specimens to intercompare the penetrabilities of selected carbonaceous shales with each other and with several

grout compositions. The objective has been to obtain a synthetic composition that more closely simulates the jet penetration characteristics of low-porosity shales. We have developed a satisfactory composition using Portland cement and ferrophosphorus sand. The density of this grout is 3.6 g/cm^3 , and the compressive strength is near 60 MPa (9000 psi). Direct axial penetration of a 10-cm- (4-in.-) diam steel-jacketed cylinder of this grout by a 32-mm-diam commercial jet perforator charge produced a shallow, conical entrance crater above a slender, uniformly tapered penetration to a depth of 195 mm

(7.7 in.), which matches that achieved in a shale specimen oriented with the penetration axis parallel to the bedding planes.

B. Dynamics of Shale Compression

Shock and particle speeds observed in our initial high-pressure planar compression wave measurements on Devonian shale core specimens² demonstrated a significant irreversible phase change at shock speeds near 6 km/s for samples oriented either parallel or perpendicular to bedding planes and for samples of both large and small organic richness. To account for this behavior in computationally modeling the hydrodynamic deformation of this rock during stimulation by direct explosive treatment or directional penetration by an explosively driven hypervelocity jet, we have had to construct formulas that systematize the Hugoniot measurements. These formulas also incorporate the pronounced strain hysteresis and high release-wave speeds that have been observed independently in certain silicate and metal-oxide minerals exhibiting the same Hugoniot behavior. Our treatment has produced algorithms that account for the pressure-induced collapse of the original polycrystalline state to a final one during an impact-and-release cycle. The model is calibrated by achieving a fit to our prior Hugoniot data and is applied in a numerical prediction of high-pressure, one-dimensional wave dynamics for Devonian shale.

C. Characterization by Laser Pyrolysis

We have conducted detailed investigations on refining laser pyrolysis and gas chromatographic techniques and applying them to selected Devonian shale core samples. To date, quantitative results are restricted to hydrocarbon products of pyrolysis that are detected by flame ionization and identified by chromatographic retention time. Using controlled loading and compacting of homogenized shale powder into pellets, we have produced satisfactory physical quality of solid samples and chromatographically determined the composition of the light hydrocarbons formed in the laser pyrolysis of the samples. We have tested the reproducibility of

absolute pyrolysis yields from shales and have determined a preliminary correlation between the absolute yield of acetylene from pulsed-laser pyrolysis and the total carbon content of a series of Devonian shales containing from 2 to 12% carbon. A conceptual design of a system for downhole application of laser pyrolysis to borehole wall material is given.

II. PENETRATION OF ROCK AND FERROPHOSPHORUS GROUT BY COPPER-CONE JETS (S. P. Marsh)

Jet penetration tests have been conducted on a variety of mineral and grout specimens using Welex* shaped charges D.P. HT-1. Radiographs of this shaped charge were presented in an earlier quarterly progress report (Ref. 1, Fig. 3). The liner is fabricated from pressed copper alloy powder and has the form of a conical shell rounded at the apex.

The cylindrical target specimens were approximately 90 mm in diameter and encased in a steel pipe with wall thickness of 6.4 mm or greater. The ends were confined by 12.7-mm-thick steel caps. None of the tests caused deformation of the steel pipes. The epoxy cement that filled the gaps between the specimen and pipe wall was not crushed or broken by the tests. The grout specimens were cast directly in the pipes, eliminating gaps. The shaped charges were fired through a 25.4-mm-diam hole in one end cap. The standoff from the shaped charge to the target specimen was the thickness of the end cap (12.7 mm).

The specimens studied in these tests are listed in Table I along with their densities, ρ . The orientation of the bedding planes of the gas shales and oil shales are indicated by (\perp) if the jet penetration was perpendicular to the planes and by (\parallel) if the penetration was parallel to the planes. The grouts selected had varying densities and yield strengths, determined by the ratio of Cal-Seal** cement, Portland cement, sand, ferrophosphorus sand, and water.

The results of the penetration tests are given in Table I. The two columns on the right indicate the

*Welex, Houston, TX 77001.

**United States Gypsum Company, Chicago, IL 60606.

TABLE I
JET PENETRATION DATA FOR MINERALS AND GROUTS

Material	ρ (g/cm ³)	Jet Penetration	
		Depth (mm)	Volume (cm ³)
Limestone, Nevada Test Site	2.72	125	6.4
Gas Shale No. 1, Lincoln County, WV (\perp)	2.53	140	---
Gas Shale No. 2, Lincoln County, WV (\perp)	2.65	150	9.6
Gas Shale No. 3, Antrim (\perp)	2.37	165	7.6
Oil Shale, Green River (\perp)	2.36	149	8.9
Oil Shale, Green River (\parallel)	2.37	200	11.2
Ferrophosphorus grouts ^a			
No. 6 (1855 psi)	3.66	213	35.7
No. 8 (2545 psi)	2.57	241	35.7
No. 12 (3570 psi)	3.58	159	28.4
No. 13 (3570 psi)	3.50	241	31.8
No. 14 (2015 psi)	3.12	187	32.1
No. 18 (8736 psi)	3.62	195	15.0
No. 21 (475 psi)	2.50	292	82.0
No. 23 (3750 psi)	2.11	305	24.2

^aCompressive yield strengths in parentheses.

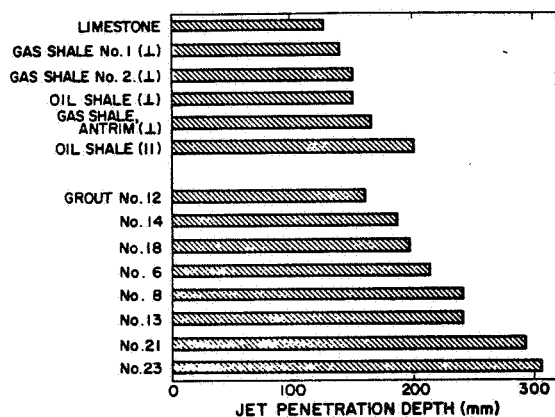


Fig. 1.
Comparison of jet penetrations into mineral and grout specimens.

depth of penetration and the volume of the penetration cavity. Figure 1 shows the comparison of the penetration depths. Photographs of some of the recovered specimens are shown in Figs. 2-5.

The least penetrable material tested was limestone, with a penetration depth of only 125 mm. The penetrations into gas shales No. 1 and No. 2 from Lincoln County, West Virginia, are greater than those into limestone by approximately 15%. The gas shale penetrations agree with each other to about 7%, which is within the variation to be expected from the shaped charges. Penetration normal to the bedding planes in oil shale agrees with penetration in the same direction into gas shales No. 1 and No. 2. However, gas shale No. 3 (Antrim) had a 14% deeper penetration than the average of those of the other gas shales, which could be a result of its higher kerogen content (indicated by its darker color and lower density).

A comparison of the two penetration directions in oil shale shows the penetration parallel to the bedding planes to be 34% deeper than the penetration normal to these planes. Because of the similarity of gas and oil shale penetrations in the direction normal to the bedding planes, we surmise that there

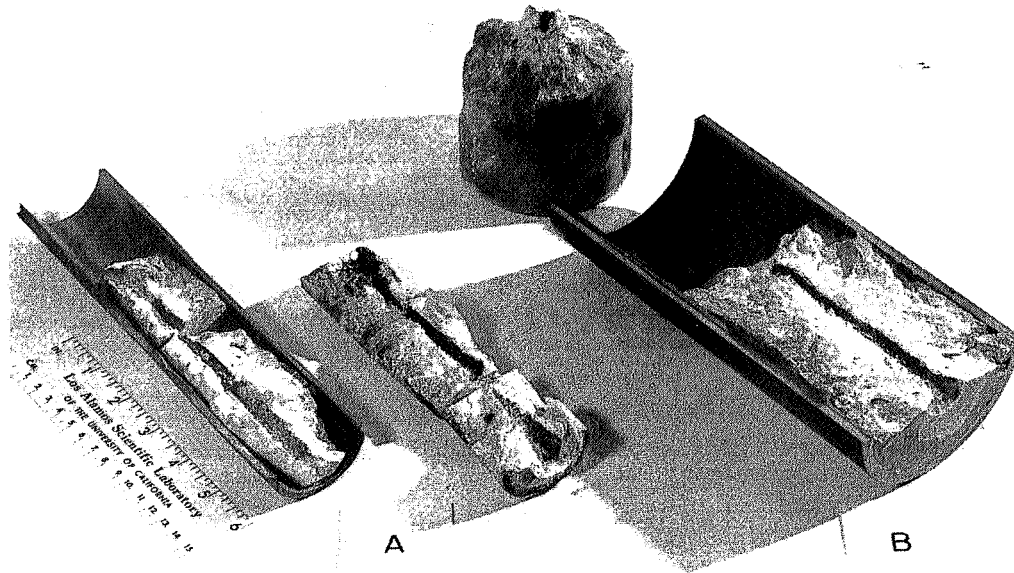


Fig. 2.

Cross sections of jet penetrations into limestone (Nevada Test Site) for (A) a 38-mm-o.d. specimen encased in a 3-mm steel pipe and (B) an 85-mm-o.d. specimen encased in a 6-mm steel pipe. Because of deformation of the specimen and pipe diameters in the small geometry, the large geometry, in which no deformation occurred, was selected. Penetration depth was 40% greater in the small, poorly confined test.

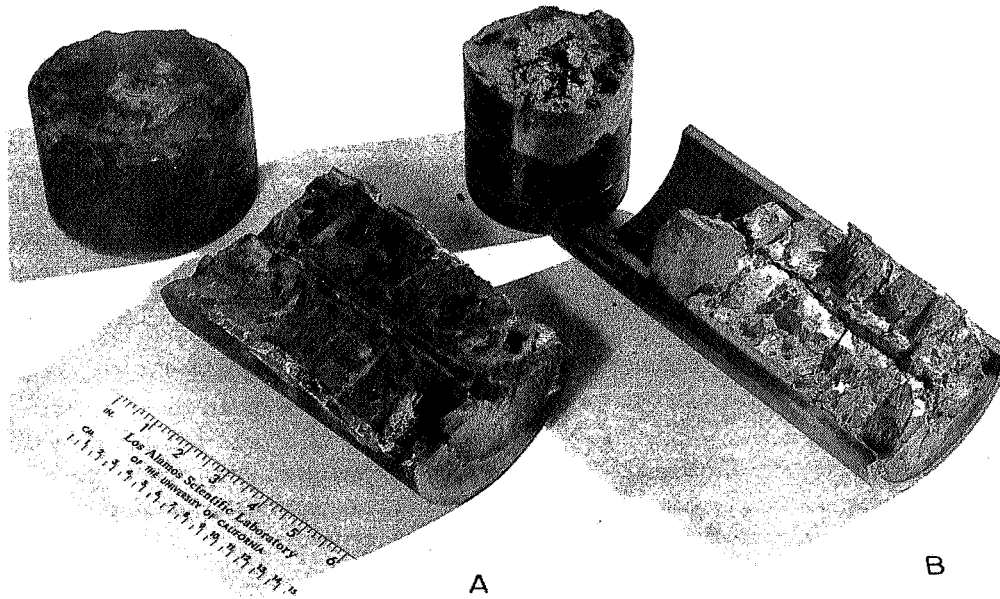


Fig. 3.

Cross sections of jet penetration into (A) gas shale No. 3 (Antrim) and (B) gas shale No. 2 (Lincoln County, West Virginia).

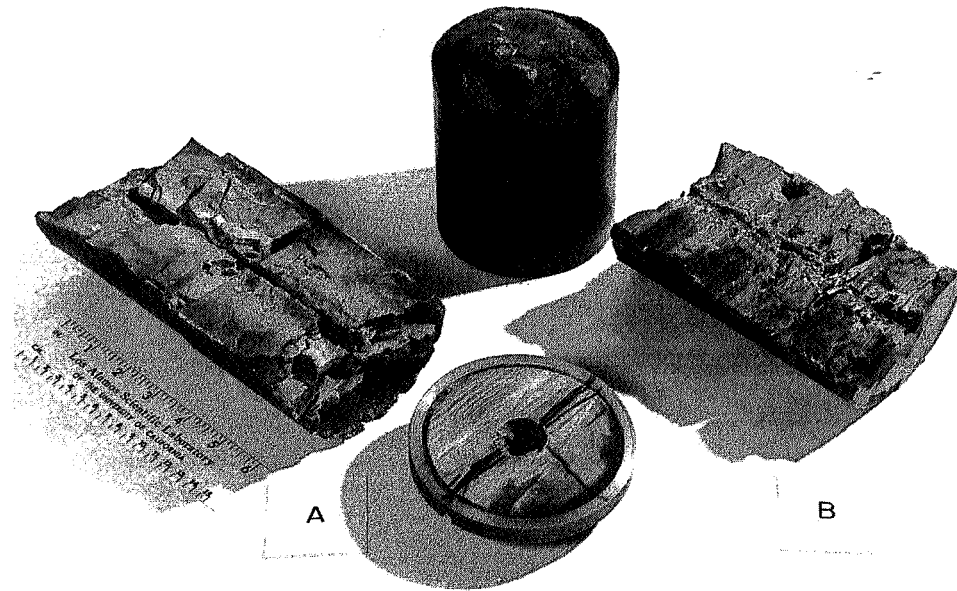


Fig. 4.
Cross sections of jet penetrations into oil shale (Green River) for (A) penetration parallel to the bedding planes and (B) penetration normal to the bedding planes.

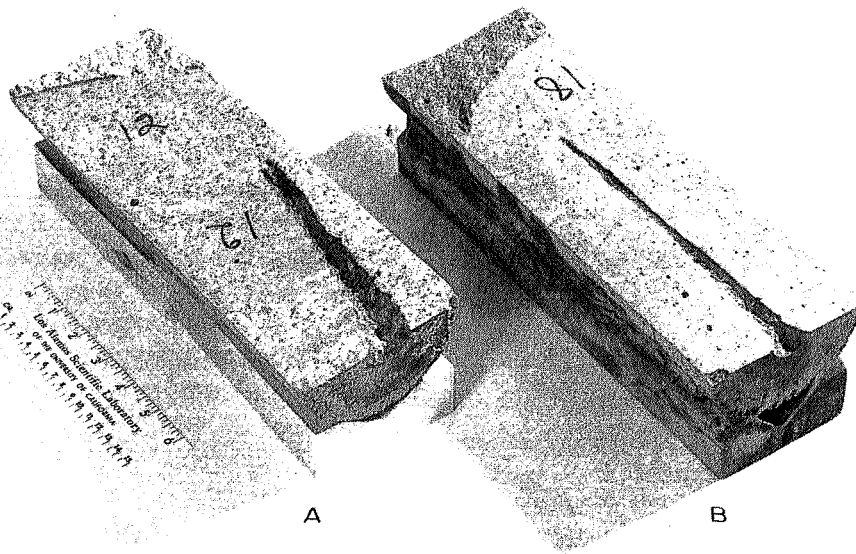


Fig. 5.
Cross sections of jet penetrations into ferrophosphorus grouts (A) No. 12 and (B) No. 18.

may also be a similarity in penetration in the direction parallel to these planes. This is the direction that gas shale would be penetrated by a jet in a gas-well stimulation test. We conclude that 200 mm is the approximate penetration parallel to the bedding planes to be expected from the shaped charges D.P. HT-1 in gas shale.

The hole volumes of these penetrations tend to be larger for the materials with deeper penetrations, which can be seen in Fig. 6.

The purpose of studying the grouts discussed here was to obtain a convenient penetration mockup of gas shale. Ferrophosphorus sand was added to increase density and decrease jet penetration so that the grouts more nearly approximate the shale specimens. Cal-Seal cement was used to obtain short cure times, but its addition resulted in lower yield strength. Portland cement was used to obtain high yield strength.

Attempts to find a mathematical relationship between the penetration depth and the yield strength and density of the grout specimens have not been successful. Work will continue on this problem.

In general, the penetration depths and hole volumes of the grouts are larger than those of the limestone and shales. However, there is an overlap in the penetration depths for grouts Nos. 12, 14, and

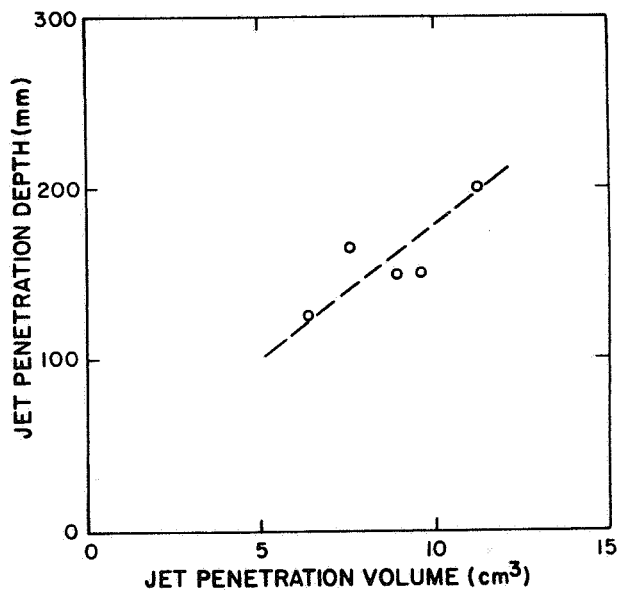


Fig. 6.

Variation of jet penetration depth with jet penetration volume for mineral specimens.

18. Grout No. 18 has a penetration depth of 195 mm, which best matches the 200-mm penetration value inferred for gas shale parallel to the bedding planes. This grout also has the smallest penetration volume (15.0 cm³), which is also the value nearest to the gas-shale hole volumes of 7.6 and 9.6 cm³. For these reasons, grout No. 18 was selected as the best penetration mockup among the grouts studied. Its formulation is given below.

Component	wt%
Ferrophosphorus sand	68.1
Portland cement	23.4
Water	8.5
LL880 ^a	0.066
(strengthening additive)	

^aMaster Builders Company, Cleveland, OH 44118.

III. DYNAMIC RESPONSE OF SHALE TO HIGH PRESSURE (J. D. Jacobson)

We describe here a simple hydrodynamic model of the typical response of rock to high-pressure impulse, namely an irreversible compaction, even in nonporous material, resulting in pronounced strain hysteresis and high release-wave speed.³⁻⁷ The extent of compaction, determined by the strength of the initial shock, is represented by a single internal-state variable that selects the pressure function as a simple Mie-Grüneisen form.

The model was devised for use in the computer simulation of hypervelocity impact in gas shales. Algorithms for evaluation of the response functions have been installed in the one-dimensional dynamics program PAD.⁸ Other algorithms have been developed to determine the material parameters from typical experimental data on the principal Hugoniot and from independent estimates of the Grüneisen coefficient. We have used these procedures to calibrate our model to a sample of Devonian gas shale,⁹ and then to simulate impact experiments of the kind required to verify our assumptions.

The model conforms to six premises about the response of nonporous rock. We now state these in an order that permits us to develop an explicit response

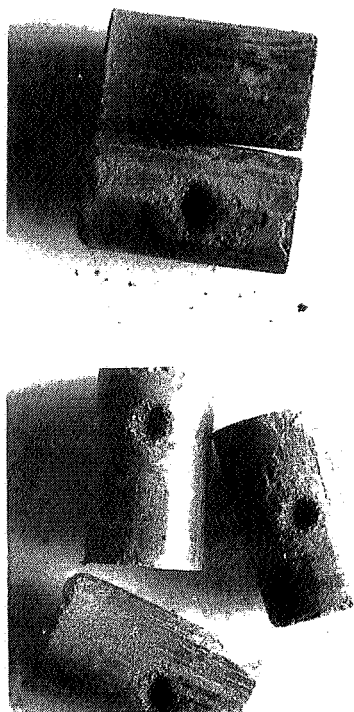


Fig. 14.

Pellets containing 90 mg of sample from the Parr press, following laser pyrolysis. Each pellet is a right cylinder, 0.32 cm in diameter and 0.56 cm high, pressed from powdered Hazard, Kentucky, core, MERC sample No. 3 [2379.6- to 2380.3-ft (725.3- to 725.5-m) depth].

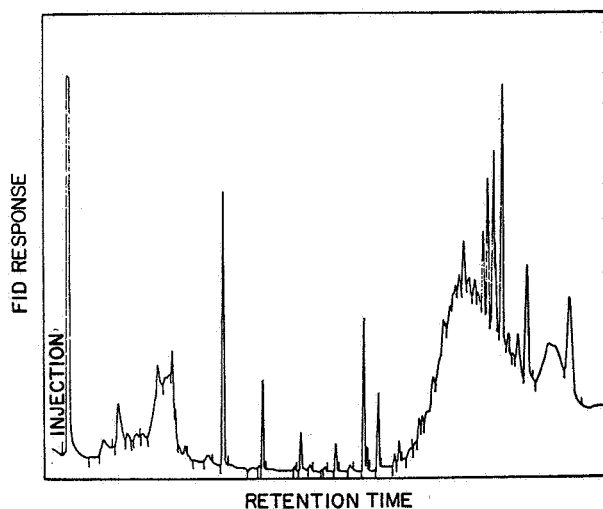


Fig. 15.

Laser pyrogram for black shale using a 1-m C₁₈ Porasil C column with temperature programming. The low-molecular-weight gas peak is the first peak following injection.

temperature programming is started and a series of compounds are detected. The large base-line shift probably results from the elution of water. We have not yet attempted to identify the compounds associated with these peaks; however, the newly acquired gas-chromatograph/mass-spectrometer combination will make this task possible.

Initial data analysis has concentrated on quantifying the low-molecular-weight gas compounds. We can readily separate those compounds appearing together in the first peak shown in Fig. 15 using a column of phenyl isocyanate bonded to Porasil C,* temperature programmed from 20 to 60°C. Injection into the column coincides with the laser pulse. Typical data are shown in Fig. 16. Here the higher molecular-weight compounds elute slowly, if at all. The FID ignores pyrolysis products other than

*Alltech Associates, Arlington Heights, IL 60004.

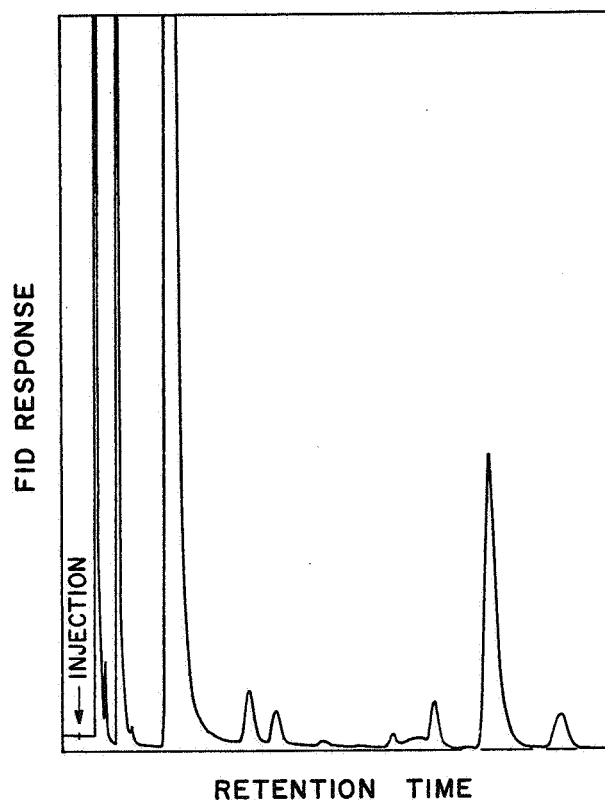


Fig. 16.

Laser pyrogram for Devonian shale sample from Perry County, Kentucky. The 1-m column of phenyl isocyanate bonded to Porasil C was temperature programmed from 20 to 60°C with no initial hold.

hydrocarbons, such as carbon dioxide, nitrogen oxides, and sulfur compounds like hydrogen sulfide. Hydrocarbons elute in the following order: methane, ethane, ethylene, propane, acetylene (the major peak in Fig. 16), propene, propyne, and then various C₄ compounds. Resolution of these compounds is excellent under these analysis conditions.

Data on replicate analyses of homogenized shale are shown in Table V. Sample pellets from the Pregl micropress were exposed to one of three successive laser shots. Data for each compound, which are listed as relative per cent and absolute integrator counts, have not been corrected for individual compound sensitivity. Because an amount of methane gives a smaller signal than an equal amount of ethane does, actual methane concentrations are approximately twice those shown in Table V.

Retention times are reproducible to ± 0.01 min because of the rapid sample production. Any poorer reproducibility than this indicates a leak. Likewise,

sharp peaks result for much the same reason. As can be seen from Table V, the relative composition in these low-molecular-weight gases is rather uniform even though the absolute amounts, as measured by the integrator counts, are more variable. (We believe that this may be due in part to inadequate temperature control of the laser cavity. Temperature control has been improved, but the quantitative effect on pyrolysis yields has not been determined.)

The composition of the low-molecular-weight gas products invariably shows an unexpectedly large methane concentration. Methane is quite unstable at the high temperatures produced during the lifetime of the plasma. Consequently, thermodynamics predicts that a vanishingly small methane concentration should result. The significant quantities we observed must result from thermal blowoff of entrapped methane and methane generated during thermal maturation caused by the

TABLE V
REPRODUCIBILITY OF LASER PYROLYSIS ON DEVONIAN SHALES^a

Compound	Retention Time (min)	Relative Per Cent of Compound ^b		
		Sample 1	Sample 2	Sample 3
CH ₄	0.50	7.43 (385 019) ^c	7.45 (465 700)	8.08 (475 149)
C ₂ H ₆	0.74	0.24 (12 354)	0.19 (12 002)	0.26 (15 527)
C ₂ H ₄	1.12	7.64 (395 923)	7.11 (444 420)	8.03 (472 021)
C ₃ H ₈	1.48	0.15 (7 562)	0.16 (10 206)	0.19 (11 464)
C ₂ H ₂	2.59	66.64 (3 452 791)	66.83 (4 176 522)	65.97 (3 878 909)
C ₃ H ₆	4.71	1.28 (66 167)	1.11 (69 546)	1.48 (85 704)
C ₃ H ₄	5.42	0.64 (33 119)	0.57 (35 451)	0.62 (36 508)
A ^d	6.60	0.24 (12 644)	0.27 (16 916)	0.26 (15 536)
B ^d	9.63	0.93 (48 041)	1.13 (70 630)	1.00 (58 538)
C ^d	10.39	4.74 (245 625)	4.25 (265 896)	4.41 (259 400)
D ^d	11.72	1.46 (75 413)	1.26 (78 675)	0.62 (36 387)
E ^d	13.84	1.34 (69 557)	1.02 (63 602)	0.86 (50 551)

^aMERC sample No. 30A, from Perry County, Kentucky, at 2509.69 to 2510.30 ft (765.0 to 765.1 m). MERC analysis: 95.75% low-temperature ash, 4.62% total carbon, 1.31% carbonate (CO₂). MERC assay: 1.4% oil (3.6 gal/ton), 1.6% water (3.8 gal/ton).

^bUncorrected for individual compound sensitivity.

^cAbsolute integrator counts in parentheses.

^dUnidentified peaks.

relation adequate for a composite as complex as shale, but that is certainly the case for the low-pressure arc of all four of the Hugoniot determined by Olinger⁹ for Devonian shale. Having accepted this form, we use the frozen Hugoniot as the reference curve $P(v, \lambda)$:

$$P(v; \lambda) = h(v_0 - v; \lambda) = h ;$$

$$E(v; \lambda) = (v_0 - v)h/2 + e_0 ;$$

$$p(v, e; \lambda) = h[1 - (v_0 - v)g/2] + (e - e_0)g .$$

(5) For sufficiently intense impact ($u > u_{II}$), the phase transitions are complete, and the high-pressure arc of the principal Hugoniot corresponds to constant λ . We will normalize λ so that

$$\Lambda(v) = \begin{cases} 0, & v \geq v_I \\ 1, & v \leq v_{II} . \end{cases}$$

Under this assumption we can determine, in principle, the five constants v_{01} , α_1 , β_1 , e_{01} , and g_1 by fitting the experimental high-pressure data to the re-centered Hugoniot $h(\Delta; 1)$; we get

$$H(\Delta) = \{h(\Delta; 1)[1 - g(\Delta - \Delta_{01})/2] - ge_{01}\} \\ \div (1 - g\Delta/2) .$$

The procedure is illustrated by several examples in Ref. 12, from which the sensitivity of the regression function to variation of the parameters can be judged. In practice, this sensitivity is too low, and the experimental data are too sparse and too scattered to permit an unequivocal determination of all five parameters by regression analysis. We expect that the Hugoniot data can be supplemented by theoretical estimates and by direct measurements on the metastable high-pressure phases when these can be prepared.

(6) There exists a mixing rule

$$\Pi = \Pi(\lambda)$$

determining the material parameters

$$\Pi = [v_0, \alpha, \beta, e_0, g] .$$

Were sufficient release-wave data available, $\Pi(\lambda)$ might be an interpolation function to the experimental data. For now we have defined $\Pi(\lambda)$ in terms of the linear operator

$$L(x) = (1 - \lambda)x_0 + \lambda x_1 ,$$

with

$$v_0 = L(v_0)$$

$$\alpha^{-2} = L(\alpha^{-2})$$

$$\beta^{-1} = L(\beta^{-1})$$

$$e_0 = L(e_0)$$

$$g^{-1} = L(g^{-1}) .$$

If λ can be regarded as the mass fraction of the high-density phase (the same for every constituent of the shale), then these equations are the rules often used for the moduli of the principal Hugoniot of an intimate mechanical mixture.¹³ The rule for β assures the ordering of the frozen asymptotes. The rule for α is that implied by treating homogeneous mixtures as the limit of certain regular laminated structures. The adoption of a mixing rule defines $\lambda = \Lambda(\hat{v})$ as the zero of the function $F(x)$, which is given by

$$F(x) = H(\hat{\Delta}) (1 - g\Delta_0/2) \\ - h(\Delta_0 - \hat{\Delta}, x)[1 - (\Delta_0 - \hat{\Delta})g/2] + ge_0 ,$$

where g , v_0 , and e_0 are functions of x , and

$$\hat{\Delta} = v_{00} - \hat{v} .$$

To illustrate the feasibility of our simple procedure, we apply it to the data of Table III and Figs. 7 and 8. They represent one of the Hugoniot determined by Olinger⁹ for a Devonian gas shale. Our least squares fits are determined by the Levenberg-Marquardt algorithm as programmed by Klein¹⁴ and Doyle.¹⁵ The fits are displayed in Figs. 7 and 8 and their parameters are listed in Table IV. That U_I should be determined by those data below $u = 1.5$ km/s is obvious, as is the acceptability of the linear form for $U_I(u)$. The choice $u_{II} \cong 3$ km/s is less obvious; its justification is that rational $U(u)$ fit to the data above this point are convex upward, which

TABLE III
HUGONIOT FOR A DEVONIAN SHALE^a

ρ_0' (g/cm ³)	u' (km/s)	U' (km/s)	$v_0' - v$ (cm ³ /g)	p' (GPa)	ρ (g/cm ³)	u (km/s)	U (km/s)	$v_{00} - v$ (cm ³ /g)	p (GPa)
2.71	0.460	4.821	0.035	6.01	2.996	0.460	4.821	0.035	6.01
2.68	0.496	4.619	0.040	6.14	3.002	0.467	4.797	0.036	6.07
2.68	0.496	4.620	0.040	6.14	3.002	0.467	4.798	0.036	6.07
2.73	0.565	4.780	0.043	7.37	3.096	0.585	4.689	0.046	7.43
2.73	0.566	4.753	0.044	7.34	3.099	0.585	4.664	0.046	7.40
2.69	0.614	4.996	0.046	8.25	3.067	0.593	5.096	0.043	8.19
2.72	0.728	5.000	0.054	9.90	3.184	0.739	4.965	0.055	9.94
2.69	0.964	5.254	0.068	13.62	3.294	0.941	5.302	0.065	13.52
2.69	0.979	5.388	0.068	14.19	3.287	0.955	5.439	0.065	14.08
2.68	0.981	5.386	0.068	14.16	3.277	0.945	5.463	0.064	13.99
2.69	1.187	5.739	0.077	18.32	3.391	1.161	5.777	0.074	18.18
2.69	1.187	5.743	0.077	18.34	3.391	1.161	5.781	0.074	18.19
2.69	1.315	5.752	0.085	20.35	3.487	1.288	5.780	0.082	20.18
2.72	1.846	6.007	0.113	30.16	3.927	1.861	6.007	0.114	30.30
2.72	1.865	5.984	0.115	30.36	3.952	1.880	5.985	0.116	30.50
2.72	1.866	5.966	0.115	30.28	3.958	1.881	5.967	0.116	30.42
2.72	2.102	6.113	0.126	34.95	4.145	2.118	6.118	0.128	35.12
2.72	2.108	6.064	0.128	34.77	4.169	2.124	6.069	0.129	34.94
2.72	2.173	6.072	0.132	35.89	4.236	2.190	6.078	0.133	36.06
2.72	2.210	6.294	0.129	37.83	4.192	2.227	6.300	0.130	38.02
2.72	2.237	6.247	0.132	38.01	4.237	2.254	6.253	0.133	38.20
2.72	2.244	6.192	0.133	37.79	4.266	2.261	6.199	0.135	37.98
2.72	2.495	6.489	0.141	44.04	4.419	2.513	6.498	0.143	44.26
2.72	2.503	6.436	0.143	43.82	4.451	2.521	6.446	0.144	44.04
2.72	2.610	6.725	0.143	47.74	4.445	2.629	6.735	0.144	47.99
2.72	2.625	6.626	0.146	47.31	4.505	2.644	6.637	0.147	47.55
2.72	2.690	6.962	0.142	50.94	4.433	2.710	6.972	0.143	51.20
2.72	2.700	6.894	0.144	50.63	4.471	2.720	6.905	0.145	50.89
2.73	2.727	6.933	0.144	51.61	4.500	2.767	6.955	0.147	52.14
2.73	2.776	6.940	0.147	52.59	4.550	2.816	6.963	0.149	53.14
2.72	3.120	7.324	0.157	62.15	4.739	3.142	7.339	0.158	62.49
2.72	3.124	7.296	0.157	62.00	4.757	3.146	7.311	0.159	62.33
2.73	3.213	7.469	0.158	65.51	4.791	3.258	7.501	0.160	66.22
2.73	3.268	7.912	0.151	70.59	4.651	3.314	7.942	0.154	71.33
2.73	3.284	7.812	0.154	70.04	4.710	3.330	7.843	0.157	70.78
2.73	3.493	7.989	0.160	76.18	4.851	3.542	8.024	0.163	77.02
2.73	3.675	8.567	0.157	85.95	4.781	3.726	8.603	0.160	86.88
2.73	3.682	8.524	0.158	85.68	4.806	3.733	8.561	0.161	86.61
2.73	3.687	8.505	0.159	85.61	4.819	3.738	8.542	0.161	86.54

^aData of Olinger (Ref. 9, Fig. 12). Primes denote experimental data for initial density $\rho_0' = 1/v_0'$. The states denoted by unprimed symbols are adjusted at the experimental shock density $\rho = 1/v$ to the average initial density $1/v_{00} = 2.71$, assuming constant $g = 1.8/v_{00}$. These corrections are not significant for this Hugoniot, and so the unadjusted values were used to give the fits of Table IV.

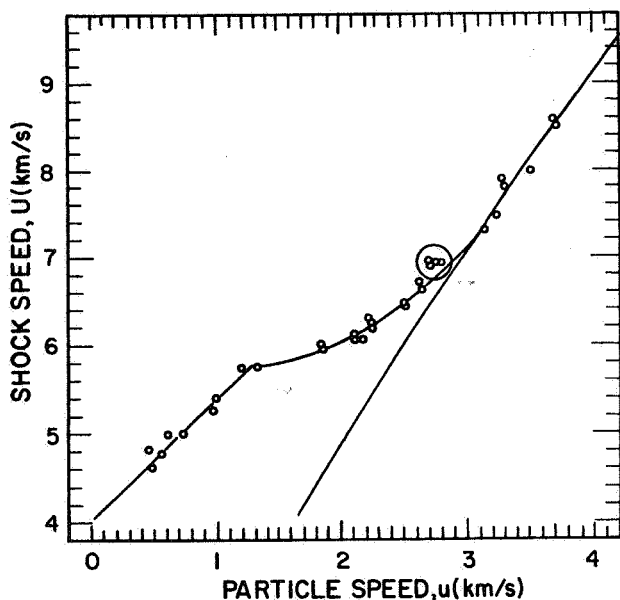


Fig. 7.

Hugoniot $U(u)$ for a sample of Devonian gas shale. Open circles are the data of Olinger (Ref. 9, Fig. 12) given in Table III. The Hugoniot is determined by the method of least squares as a curve of three segments. The upper segment is the hypothetical Hugoniot of complete phase conversion centered on the experimental initial state; it is shown extrapolated to speeds below those experimentally accessible. The circled four points in the center segment are thought to be off the metastable Hugoniot and are not included in the fit.

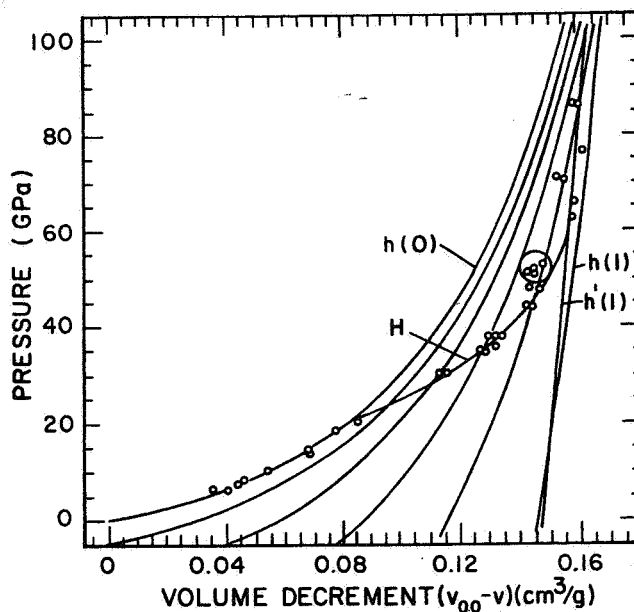


Fig. 8.

Hugoniots $p(v_{00} - v)$ for a sample of Devonian gas shale (projection of Fig. 7). Open circles are the data of Olinger.⁹ Curve H is the least squares fit to the experimental data. Curve $h(0)$ is the principal Hugoniot for constant phase composition $\lambda = 0$. Curve $h(1)$ is the principal Hugoniot for constant phase composition $\lambda = 1$. Curve $h'(1)$ is the Hugoniot $h(1)$ re-centered at the experimental initial state with $g = g_1$. Also shown are the principal Hugoniots for $\lambda = 0.2, 0.4, 0.6,$ and 0.8 .

TABLE IV

MATERIAL PARAMETERS FOR
FIGS. 7 AND 8

λ	v_0^{-1} (g/cm ³)	$v_0\alpha$ (km/s)	$v_0\beta$	e_0 (J/kg)	v_0g
0	2.71	4.024	1.38	0	1.00
1	4.47	13.565	1.20	0.8	1.80

$$U_{II}(u) = (6.2768 - 0.9778 u + 0.3929 u^2)/(1 - 0.01252 u) \text{ km/s}$$

$$u_I = 1.2577 \text{ km/s}$$

$$u_{II} = 3.0620 \text{ km/s}$$

is the theoretical form under our assumptions. Including in the fit one or more of the first five points below $u = 3$ km/s spoils this agreement. We estimated g and e_{01} , as explained below, leaving the three parameters v_{01} , α_1 , and β_1 to be determined by the fit to $H(\Delta)$. Convergence was very slow, and the merit functions supplied by the program could not distinguish values of $v_{01}\beta_1$ in the range (1.1, 1.5). The value $v_{01}\beta_1 = 1.2$ was fixed to give the two-parameter fit shown in Fig. 7. With these breakpoints, reasonable fits (cubic polynomial and quadratic/linear rational) to $U_{II}(u)$ fail to intersect $U_{II}(u)$. Rather than accepting another round of compaction and the associated two-wave response, we propose that an endothermic relaxation intrudes at $p \cong 50 \times 10^9$ Pa, $U \cong 7$ km/s. Then, as observed, the cluster of four points just below $u = u_{II}$ would be high in U and low in u compared to the equilibrium

Hugoniot. On this basis, we leave those data out of the mixed-phase group, which is then fit satisfactorily by a rational function.

We follow a common practice in choosing g to be a constant function of v . The value selected for g_0 is not quite arbitrary; instead it is based on a comparison of this Hugoniot with the other determined by Olinger at the same average initial density but with a different direction of impact relative to the shale grain. Our assumption of fluid response suggests that the two Hugoniots should agree at the pressures of the experiments. Such an agreement is realized when a value $g_0 = 1.8/v_{00}$ is used to correct for deviations of the initial density from its average value. The value of $g_1 = 1/v_{01}$ is that estimated for stishovite,¹⁶ the high-pressure phase of quartz, which is a major constituent of the shale. Likewise, the value chosen for the energy of transformation, $e_{01} = 0.8$ MJ/kg, is an estimate for the quartz-stishovite transformation.¹⁶

We note that the values of v_{00}/v_{01} and α_1/α_0 are close to those for the quartz-stishovite system,¹⁶ suggesting that all of the constituents of shale undergo similar phase transformations. We know of no experiments that could directly confirm this conclusion for the anhydrous clays, which constitute about 50% of the shale.

To illustrate the effect of the irreversible compaction on wave propagation, we have used the program PAD to compute the attenuation of a square pressure pulse of 50×10^9 Pa, $1 \mu\text{s}$ in duration, in the material of our example. The history at a particle traversed by the wave is shown in Fig. 9. For comparison, we show the effect of the same load applied to the same material except that the principal Hugoniot is taken to be one of equilibrium. It is plausible that compaction phenomena of the kind treated here should have a significant role in the jet penetration of shale.

IV. PULSED-LASER PYROLYSIS (N. E. Vanderborgh and J. P. Bertino)

The Los Alamos Scientific Laboratory (LASL) program in Devonian shale characterization uses a pulsed laser to rapidly heat a localized shale sample. Product gases are collected and inserted into an on-line gas chromatograph. The objective of our experiments is to develop rapid, quantitative survey

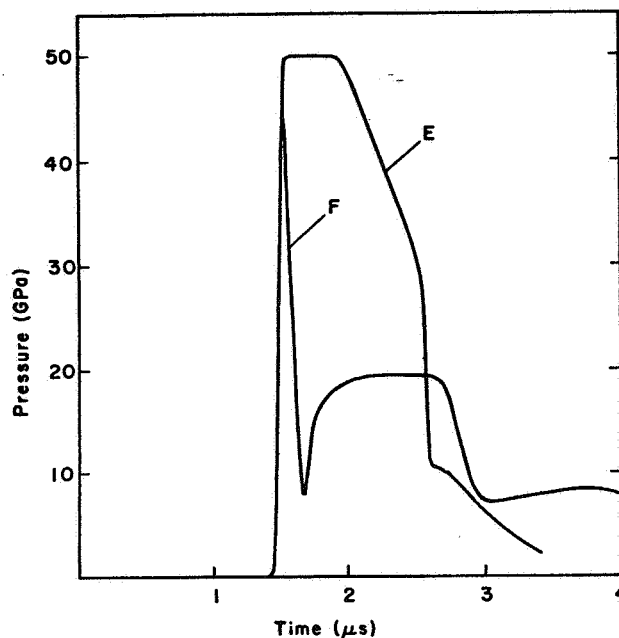


Fig. 9.

The history of pressure at a particle 10 mm from an interface held at 50 GPa for $1 \mu\text{s}$ beginning at time $t = 0$. The material model is the example discussed in the text. Curve F is frozen unloading; curve E is equilibrium unloading.

methods that measure the organic chemical composition in various shale samples. Progress during this quarter has concentrated on comparing laser pyrolysis results with analytical data obtained from Morgantown Energy Research Center (MERC) on particular core sections removed from Devonian shale in Kentucky.

A. General Approach

The experimental arrangement for these measurements is shown in Fig. 10. We use a neodymium-doped glass laser system that works in the normal burst mode. Energy at $1.06 \mu\text{m}$ with a pulse length of 0.001 s is deposited into a shale sample contained in a quartz sample tube. Short but intense pyrolysis occurs within a flowing carrier gas stream that transfers pyrolysis products from the sample into the gas chromatograph. Two different types of product are formed by this process.

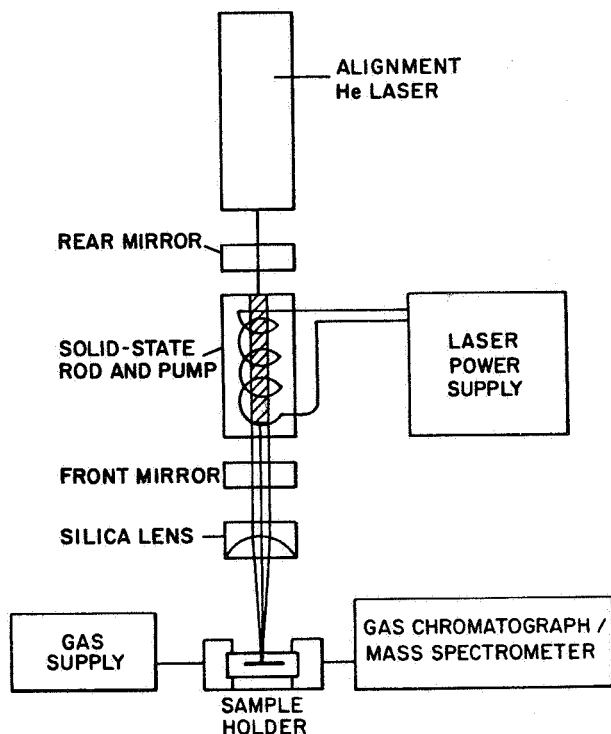


Fig. 10.

Laser pyrolysis instruments used for the rapid characterization of Devonian shale samples.

Figure 11 shows a schematic representation of the laser pyrolysis process. Here, 2 to 10 J of pulsed laser energy are deposited into a particular sample region. Part of the energy is absorbed. Usual spectroscopic processes are not influenced by such low-energy photons; however, either through multiphoton absorption or through electron tunneling, a cluster of surface atoms is ionized. This ionized cluster moves into the direction of the laser beam forming a high-temperature plasma. Because the electron absorption of energy is far more efficient (by $\sim 10^4$) than similar ion absorption, the laser energy is efficiently coupled into the free-electron cloud. Also, because of the high temperatures ($>10^4$ K) and reasonably high pressures [>133 kPa (1000 torr)], heat transfer within the plasma is rapid. As a result, we can assume that the molecular fragments in the plasma are in the kinetic equilibrium that can be described as an isothermal environment. During the last part of the pyrolysis, the high plasma absorption efficiency effectively shields the sample from the laser beam. However, the high plasma temperature sug-

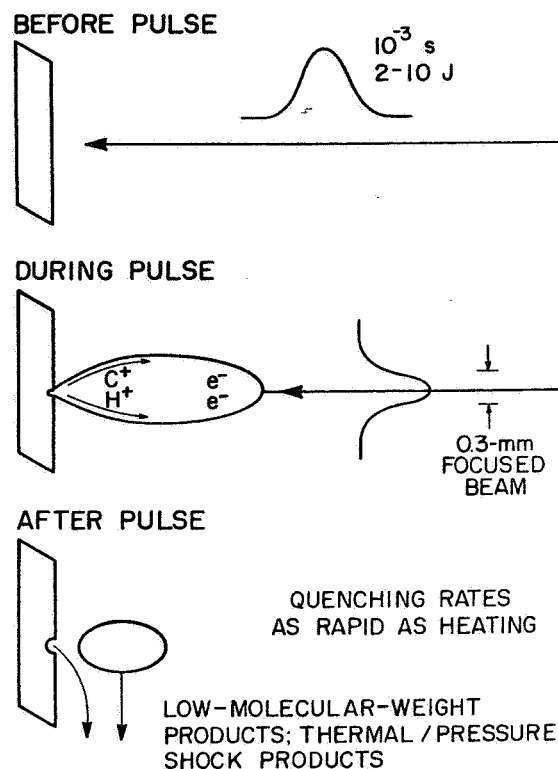


Fig. 11.

Laser pyrolysis product mechanisms.

gests that this plasma serves as a blackbody radiator, which locally heats the sample, pumping additional material into the gas phase.

At the end of pyrolysis, the entire system quenches to ambient conditions. Atoms in the plasma combine to form low-molecular-weight gases. Thus, for these shale samples, the hydrocarbon gas acetylene, C_2H_2 , is formed. Ample data suggest that these compounds are formed under equilibrium conditions at an elevated temperature near 3500 K. This is not the peak temperature of the pyrolysis process but that temperature reached during the quenching process that couples the unbound electrons (highly effective heat transfer agents) into atomic manifolds. Without the possibility of further rapid heat transfer, molecular equilibrium at that elevated temperature is "frozen" into the low-molecular-weight distribution. Consequently, the makeup of those gases reflects the atomic composition of the plasma.

Some of the energy generated from ion-electron recombination in the plasma penetrates the sample beneath, leading to the formation of a second type of product that we call thermal/pressure shock products. They are compounds of higher molecular weight than most of the plasma-formed products, compounds that are characteristic of the larger molecular fragments in the pyrolysis sample.

Laser-induced pyrolysis offers unusual flexibility in pyrolysis/chromatography. Foremost is the energy density of the laser. Unfocused beam deposition (diameter of 0.95 cm) seldom causes appreciable effect; highly focused pyrolysis produces a high concentration of plasma-produced compounds. We usually optimize between these two extremes, typically by running the pyrolysis with the sample surface slightly closer to the focusing lens than the point of focus. Control involves carefully positioning the sample so that the distance between the lens and the sample surface is reproduced each time. The laser output can also be varied. We can vary the length of the event by changing the inductance of the capacitor bank and vary the total power by changing the charging voltage. With careful control, we can reproduce both the pulse shape and absolute power within $\pm 5\%$.

It may not be possible to completely reproduce sample energy deposition on shale samples. Although the laser parameters can be controlled, heating of the sample is not as straightforward. Accurately estimating total absorbed energy is difficult. Part of the pulse energy can be reflected and part radiated. Energy concentration depends upon thermal diffusivity. Samples such as crystalline solids do not form appreciable product because the rapid heat flow precludes a significant temperature rise. For these solids, it may be necessary to first heat the sample to a temperature higher than ambient but not high enough to cause pyrolysis.

B. Sample Preparation

Data have been collected on sample preparation methods. Two different types of samples are being used for our shale studies. In one type, homogenized powders are pressed into pellets of uniform consistency. The other samples are chips of original shale either from a drilling operation or from coarse crushing.

A fixed, low-wattage (2.5 mW) helium-neon alignment laser is used to locate the pyrolysis spot. This laser is mounted on the same optical bench that contains the optics for the main neodymium laser and is coaxial with the main system. The highly collimated beam thus illuminates the exact spot that will be pyrolyzed. Inaccurate positioning would cause the laser beam to "miss" the small solid samples. Figure 12 illustrates the precision of the positioning achieved with this device. Each of the two small chips, formed by crushing a shale core section, is approximately 0.5 by 0.2 by 0.1 cm. Craters (~ 0.06 cm in diameter) from pyrolysis on the smallest dimension are readily visible. This precision in selecting sampling locations will be important when we study the spatial variations of organic composition along particular regions of shale samples.

Close inspection of the craters in Fig. 12 also showed that the surface left after laser pyrolysis of these shale chips is covered with a whitish powder, probably quartz, and droplets, probably organic liquids released during the rapid thermal shock and then condensed on the surface.

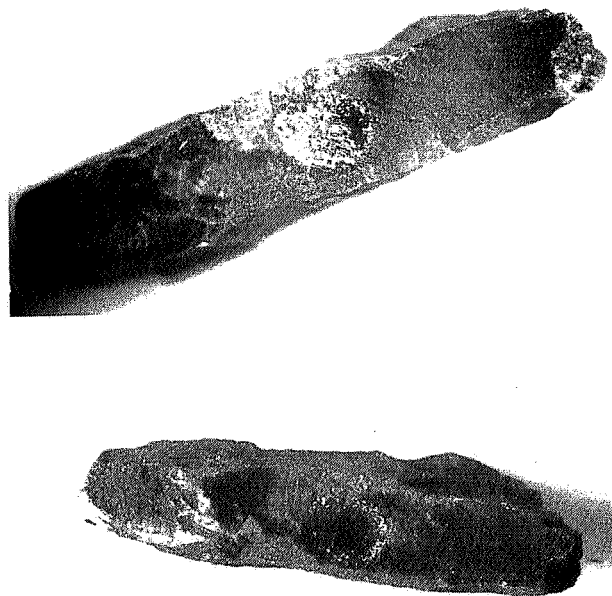


Fig. 12.
Photomicrographs of shale chips showing laser-produced craters following pyrolysis. These samples are approximately 0.5 cm long and 0.1 cm high.

A series of experiments was completed to test various parameters of powdered samples. Initially, we pelletized the powdered shale with a Pregl micropellet press;* most of the chromatographic analysis results presented in this section were obtained with such pellets. However, the uniformity of the pellet densities is questionable, because of the lack of control in applying pelletizing pressure. Thus we tried another pelletizing press, manufactured by Parr Instruments,** which produces pellets of 0.318-cm diameter as supplied. It could make pellets of controlled density, because a cam-lever arrangement moves the punch a fixed distance into the die. If a constant amount of sample is introduced, then uniform density should be achieved. To vary the densities we simply start with different quantities of sample.

Photomicrographs of several pellets prepared from the same batch of powdered shale [Hazard, Kentucky, core, sample No. 20, 2460.0- to 2460.6-ft (749.8- to 750.0-m) depth] are shown in Fig. 13. Figure 13A shows typical pellets produced by the Pregl micropress. Low-power microscopic examination shows this pellet consists of a poorly consolidated surface covering a center core that appears to be much like the bulk sample; that is, a skin of higher density material is formed around the original sample. Figure 13B shows a pellet produced with the Parr press using 85 mg of sample. This pellet is 0.318 cm in diameter and 0.562 cm high. The resulting mean density is 1.90 g/cm³, well below the bulk density of the original shale core sample. This pellet configuration was easily formed; however superficial cracks are obvious.

Increasing the powder quantity to 90 mg produced pellets of density 2.01 g/cm³ (Fig. 13C). Although slightly more force was necessary to press the sample to this density, the pellet was easily removed from the die. The appearance of the surface was far more compacted than that of the Fig. 13B pellet. However, dissection revealed again that a skin of consolidated material covers an interior of less compacted sample.

It was possible to increase the pellet density to 2.24 g/cm³ using the Parr press to compact 100 mg of powder. Although the punch was brought into a fully down position with this much material, it was dif-

ficult to remove the pellet from the die, and a certain amount of surface damage occurred (Fig. 13D). This pellet showed uniform compaction through the pellet, however.

We decided to press the 100-mg sample to a pressure of 10 000 psi (69 MPa) using a hydraulic press and an available punch and die. The density of these pellets (Fig. 13E) was somewhat higher than the values for the others in Fig. 13A-13D. Upon visual inspection, these pellets were judged to be more uniform than any prepared using the Parr press.

Each of these types of sample was used for laser pyrolysis. A photomicrograph of the resulting craters in pellets prepared by the Parr press is shown in Fig. 14. Visual inspection shows that these craters are considerably deeper than those found on small chips of shale. Obviously, some ablation of the surface results as gases are generated in the interior. Although the total volume of gases generated by the laser pulse was not constant (the laser was not operating at a constant temperature), the apparent volume removed from the sample is approximately constant. The condensed droplets around the rim of each laser-induced crater appear to be of the same material found around the solid-sample craters.

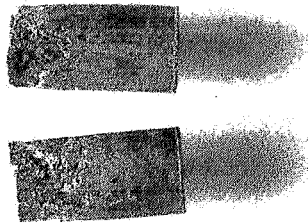
Analysis of pyrolysis data from the series of pellets in Fig. 13 shows that acetylene yield increased toward a maximum for pellets of higher density. Probably the more dense material maintains a higher heat concentration in the solid sample, which results in higher acetylene concentrations. Data from Pregl pellets showed ~60% acetylene; data from the Parr pellets showed ~71% acetylene. (This is the uncorrected value for integrator counts of the low-molecular-weight gases.) Similar results were obtained for the high-density pellet from the static press. Consequently, we concluded that compacting pellets to a density of ~2.0 g/cm³ (90 mg of sample) yields a consistent sample with a minimum of experimental difficulty.

C. Chromatography

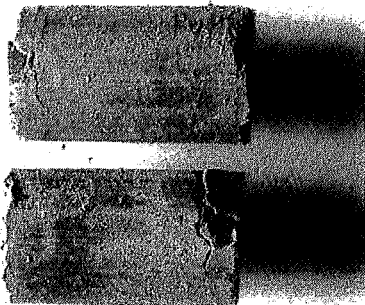
Data have been collected from 25 samples of shale supplied by MERC workers. Figure 15 shows a typical chromatographic data trace obtained with a flame ionization detector (FID) using a C₁₈ column. The low-molecular-weight gases, here poorly resolved, elute together as the first peak. Then

*Arthur H. Thomas Company, Philadelphia, PA 19105.

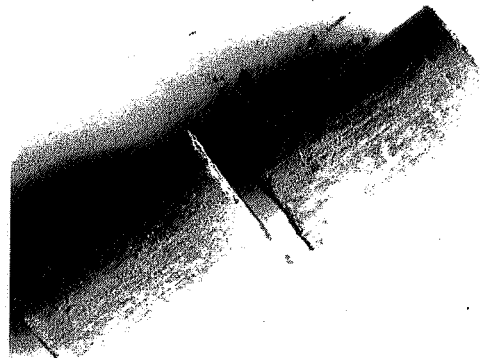
**Parr Instrument Company, Moline, IL 61265.



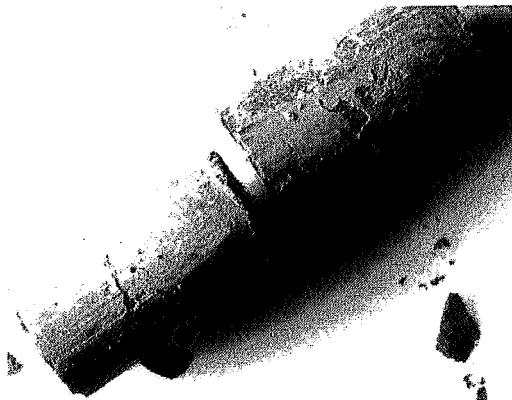
(A) Pellets from the Pregl micropress.



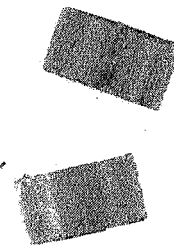
(B) Pellets from the Parr press with 85 mg of sample.



(C) Pellets from the Parr press with 90 mg of sample.



(D) Pellets from the Parr press with 100 mg of sample.



(E) Pellets prepared to high density using a static press at 10 000 psi (69 MPa).

Fig. 13.

Pellets for laser pyrolysis pressed from powdered Devonian shale from Kentucky-West Virginia Gas Co. Well No. 7239, Perry County, Kentucky, 2460.0- to 2460.6-ft (749.8- to 750.0-m) depth.

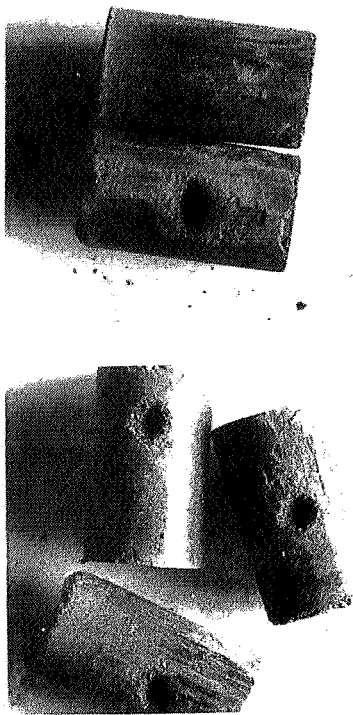


Fig. 14.

Pellets containing 90 mg of sample from the Parr press, following laser pyrolysis. Each pellet is a right cylinder, 0.32 cm in diameter and 0.56 cm high, pressed from powdered Hazard, Kentucky, core, MERC sample No. 3 [2379.6- to 2380.3-ft (725.3- to 725.5-m) depth].

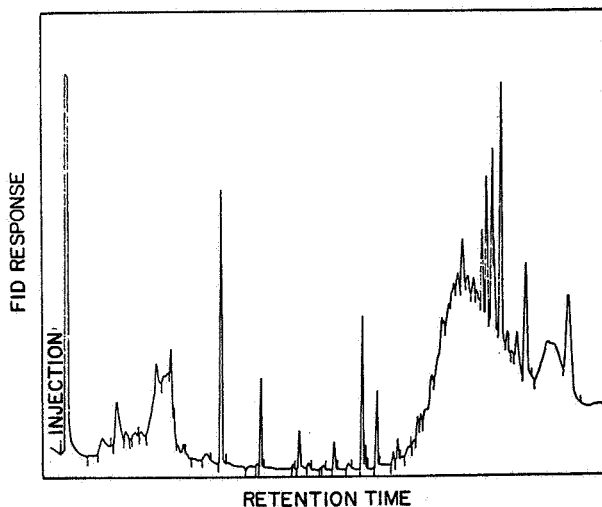


Fig. 15.

Laser pyrogram for black shale using a 1-m C₁₈ Porasil C column with temperature programming. The low-molecular-weight gas peak is the first peak following injection.

temperature programming is started and a series of compounds are detected. The large base-line shift probably results from the elution of water. We have not yet attempted to identify the compounds associated with these peaks; however, the newly acquired gas-chromatograph/mass-spectrometer combination will make this task possible.

Initial data analysis has concentrated on quantifying the low-molecular-weight gas compounds. We can readily separate those compounds appearing together in the first peak shown in Fig. 15 using a column of phenyl isocyanate bonded to Porasil C,* temperature programmed from 20 to 60°C. Injection into the column coincides with the laser pulse. Typical data are shown in Fig. 16. Here the higher molecular-weight compounds elute slowly, if at all. The FID ignores pyrolysis products other than

*Alltech Associates, Arlington Heights, IL 60004.

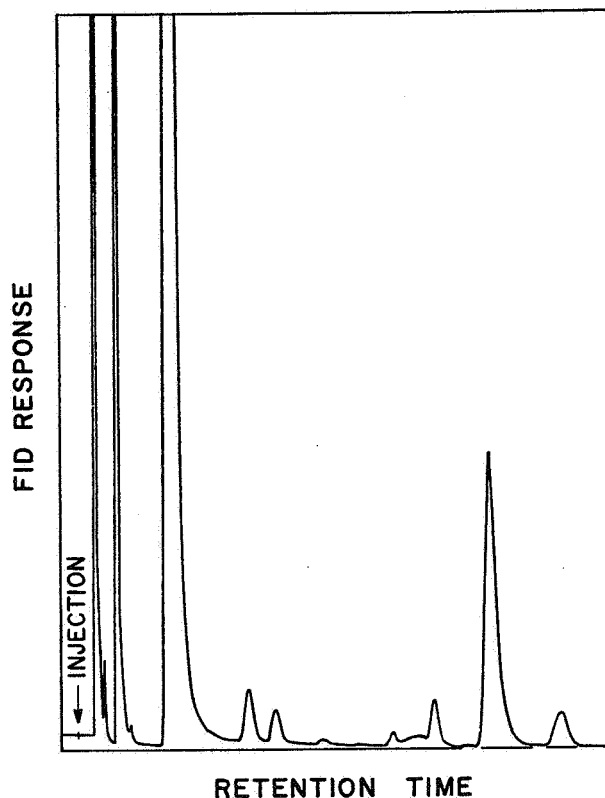


Fig. 16.

Laser pyrogram for Devonian shale sample from Perry County, Kentucky. The 1-m column of phenyl isocyanate bonded to Porasil C was temperature programmed from 20 to 60°C with no initial hold.

hydrocarbons, such as carbon dioxide, nitrogen oxides, and sulfur compounds like hydrogen sulfide. Hydrocarbons elute in the following order: methane, ethane, ethylene, propane, acetylene (the major peak in Fig. 16), propene, propyne, and then various C₄ compounds. Resolution of these compounds is excellent under these analysis conditions.

Data on replicate analyses of homogenized shale are shown in Table V. Sample pellets from the Pregl micropress were exposed to one of three successive laser shots. Data for each compound, which are listed as relative per cent and absolute integrator counts, have not been corrected for individual compound sensitivity. Because an amount of methane gives a smaller signal than an equal amount of ethane does, actual methane concentrations are approximately twice those shown in Table V.

Retention times are reproducible to ±0.01 min because of the rapid sample production. Any poorer reproducibility than this indicates a leak. Likewise,

sharp peaks result for much the same reason. As can be seen from Table V, the relative composition in these low-molecular-weight gases is rather uniform even though the absolute amounts, as measured by the integrator counts, are more variable. (We believe that this may be due in part to inadequate temperature control of the laser cavity. Temperature control has been improved, but the quantitative effect on pyrolysis yields has not been determined.)

The composition of the low-molecular-weight gas products invariably shows an unexpectedly large methane concentration. Methane is quite unstable at the high temperatures produced during the lifetime of the plasma. Consequently, thermodynamics predicts that a vanishingly small methane concentration should result. The significant quantities we observed must result from thermal blowoff of entrapped methane and methane generated during thermal maturation caused by the

TABLE V
REPRODUCIBILITY OF LASER PYROLYSIS ON DEVONIAN SHALES^a

Compound	Retention Time (min)	Relative Per Cent of Compound ^b		
		Sample 1	Sample 2	Sample 3
CH ₄	0.50	7.43 (385 019) ^c	7.45 (465 700)	8.08 (475 149)
C ₂ H ₆	0.74	0.24 (12 354)	0.19 (12 002)	0.26 (15 527)
C ₂ H ₄	1.12	7.64 (395 923)	7.11 (444 420)	8.03 (472 021)
C ₃ H ₈	1.48	0.15 (7 562)	0.16 (10 206)	0.19 (11 464)
C ₂ H ₂	2.59	66.64 (3 452 791)	66.83 (4 176 522)	65.97 (3 878 909)
C ₃ H ₆	4.71	1.28 (66 167)	1.11 (69 546)	1.48 (85 704)
C ₃ H ₄	5.42	0.64 (33 119)	0.57 (35 451)	0.62 (36 508)
A ^d	6.60	0.24 (12 644)	0.27 (16 916)	0.26 (15 536)
B ^d	9.63	0.93 (48 041)	1.13 (70 630)	1.00 (58 538)
C ^d	10.39	4.74 (245 625)	4.25 (265 896)	4.41 (259 400)
D ^d	11.72	1.46 (75 413)	1.26 (78 675)	0.62 (36 387)
E ^d	13.84	1.34 (69 557)	1.02 (63 602)	0.86 (50 551)

^aMERC sample No. 30A, from Perry County, Kentucky, at 2509.69 to 2510.30 ft (765.0 to 765.1 m). MERC analysis: 95.75% low-temperature ash, 4.62% total carbon, 1.31% carbonate (CO₂). MERC assay: 1.4% oil (3.6 gal/ton), 1.6% water (3.8 gal/ton).

^bUncorrected for individual compound sensitivity.

^cAbsolute integrator counts in parentheses.

^dUnidentified peaks.

pyrolysis process. If we could show that the latter process generated insignificant quantities of methane under our experimental conditions, then we might use the methane "yield" as a convenient measure of the gas production potential for any particular shale zone. This possibility will be explored.

Rather obviously, higher carbon content should yield larger quantities of low-molecular-weight gaseous products. Such comparisons are complicated by the fact that absolute quantities of gas are influenced by sampling irreproducibility. However, we did compare data taken from averaged yields of acetylene (three separate analyses of each material were averaged) produced during laser pyrolysis with data generated by MERC using more conventional techniques (Fig. 17). The relative deviation of each sample from the plotted mean was ~15%, but the average values, plotted in Fig. 17, do not deviate this much from the smooth curve. Because these particular samples have relatively low carbonate content, the total and organic carbon contents are approximately the same. Although this sort of correlation is preliminary, it does use the acetylene yield, a value that can be rapidly measured because acetylene has a short retention time. This analysis of acetylene yield, which ignores the other products of laser pyrolysis, can be done in less than 1 min.

Such a correlation strongly suggests that laser pyrolysis, with minimal sample preparation, offers a

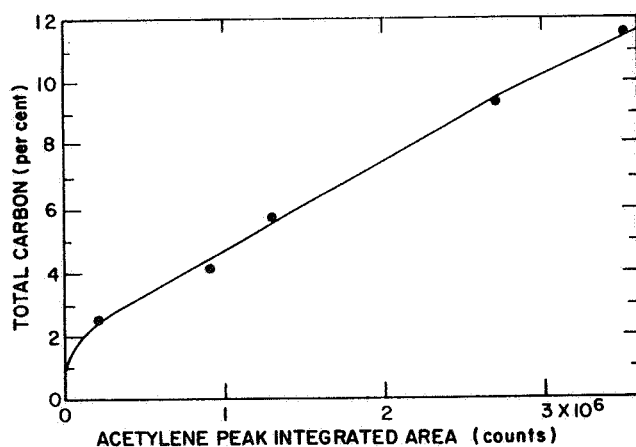


Fig. 17.

Correlation between acetylene yield (absolute counts) obtained with laser pyrolysis on Devonian shale samples from powdered Hazard, Kentucky, cores and total carbon data (MERC) from the same cores.

simplified technique for the rapid characterization of shale for carbon content. This is the first purpose of the LASL project in laser pyrolysis. It would seem possible that such measurements could be done readily in the field either on drilling chips or on the wall of an uncased hole.

D. Tool Design

The conceptual design of a tool for making downhole measurements is shown in Fig. 18. After bore cleaning, this tool is jacked against a particular wall section, isolating an area of the section with a rubber seal. (We assume that the bore is not fractured, typical for shale wells.) The isolated region is then flushed with inert (carrier) gas. When pressurization in the pyrolysis region indicates that there are no leaks, the laser is remotely fired. A focusing mirror is used to both turn and focus the beam so that a proper energy concentration is deposited through a quartz rod into the sample. Pyrolysis products are injected into a small chromatographic column operating at fixed temperature. Data are

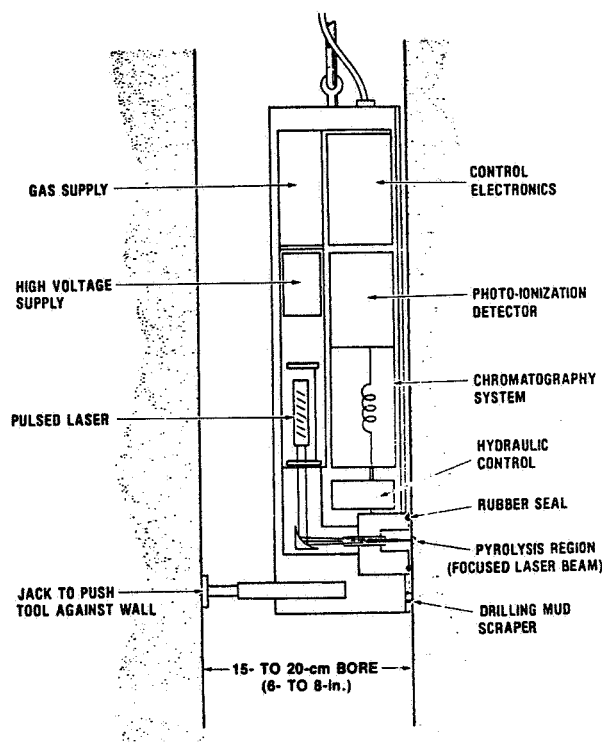


Fig. 18.

Downhole pyrolysis/gas-chromatography logging tool for in situ chemical characterization.

determined using a photo-ionization detector, a device that is somewhat less sensitive than the more usual FID but does not depend upon a hydrogen flame to cause ionization. Data are electronically transmitted to aboveground recording equipment. After analyzing a particular horizon, the tool position is changed and data are again determined.

Such field measurement is the long-range goal of the LASL project in support of the Eastern Gas Shales Project. It is becoming apparent that customized stimulation treatments of gas wells will require good characterization of the particular geologic horizon which must be treated. Downhole geochemical instruments, such as the ones shown in Fig. 18, represent one way to improve understanding of deeply lying geological formations.

REFERENCES

1. G. L. Schott, Compiler, "Stimulation and Characterization of Eastern Gas Shales, July—September 1977," Los Alamos Scientific Laboratory report LA-7320-PR (June 1978).
2. W. J. Carter and N. E. Vanderborgh, Compilers, "Evaluation of Methods for Stimulation and Characterization of Eastern Gas Shales, April—June 1977," Los Alamos Scientific Laboratory report LA-7094-PR (January 1978).
3. T. J. Ahrens and J. T. Rosenberg, "Shock Metamorphism: Experiments on Quartz and Plagioclase," in *Shock Metamorphism of Natural Materials*, B. M. French and N. M. Short, Eds. (Mono Book Company, Baltimore, 1968), p. 59.
4. D. E. Grady, W. J. Murri, and G. R. Fowles, "Quartz to Stishovite: Wave Propagation in the Mixed Phase Region," *J. Geophys. Res.* **79**, 332 (1974).
5. D. E. Grady, W. J. Murri, and P. S. De Carli, "Hugoniot Sound Velocities and Phase Transformations in Two Silicates," *J. Geophys. Res.* **80**, 4857 (1975).
6. D. E. Grady, W. J. Murri, and K. D. Mahrer, "Shock Compression of Dolomite," *J. Geophys. Res.* **81**, 889 (1976).
7. T. J. Ahrens, D. L. Anderson, and A. E. Ringwood, "Equations of State and Crystal Structures of High-Pressure Phases of Shocked Silicates and Oxides," *Rev. Geophys.* **7**, 667 (1969).
8. W. Fickett "PAD, A One-Dimensional Lagrangian Hydrocode," Los Alamos Scientific Laboratory report LA-5910-MS (April 1975).
9. B. W. Olinger, "Dynamic Properties of Devonian Shales," in "Evaluation of Methods for Stimulation and Characterization of Eastern Gas Shales, April—June 1977," W. J. Carter and N. E. Vanderborgh, Compilers, Los Alamos Scientific Laboratory report LA-7094-PR (January 1978).
10. D. E. Grady, "Processes Occurring in Shock Wave Compression of Rocks and Minerals," in *High Pressure Research: Applications in Geophysics*, M. Manghnani and S. Akimoto, Eds. (Academic, New York, 1977), p. 389.
11. G. E. Duvall, Chap. 4 in *Dynamic Response of Materials to Intense Impulsive Loading*, P. C. Chou and A. K. Hopkins, Eds. (Air Force Materials Laboratory, Wright-Patterson AFB, Ohio, 1972).
12. R. G. McQueen, S. P. Marsh, and J. N. Fritz, "Hugoniot Equation of State of Twelve Rocks," *J. Geophys. Res.* **72**, 4999 (1967).
13. S. K. Garg and J. W. Kirsch, "Hugoniot Analysis of Composite Materials," *J. Compos. Mater.* **5**, 428 (1971).
14. M. M. Klein, "Experiences in Least Squares Optimization in the LASL Environment," Los Alamos Scientific Laboratory internal document, 1972.
15. T. C. Doyle, "Nonlinear Least Squares Optimization of a Continuous N-Parameter System," Los Alamos Scientific Laboratory internal document, 1972.
16. T. J. Ahrens, T. Takahashi, and G. F. Davies, "A Proposed Equation of State of Stishovite," *J. Geophys. Res.* **75**, 310 (1970).

Distribution

US Department of Energy
Office of Fossil Energy
Washington, DC 20545
Attn: George Fumich, Prog. Director
Director, Division of Fossil

Fuel Extraction
W. B. Schmidt
A. M. Hartstein
J. Ham
D. C. Ward
J. B. Smith
A. B. Crawley

US Department of Energy
Morgantown Energy Technology Center
P.O. Box 880
Morgantown, WV 26505
Attn: A. A. Pitrolo, Director
L. A. Schrider
R. L. Wise
W. K. Overbey, Jr.
A. E. Hunt
C. A. Komar

Bartlesville Energy Technology Center
P.O. Box 1397
Bartlesville, OK 74003
Attn: Director

Laramie Energy Technology Center
P.O. Box 3395, University Station
Laramie, WY 82071
Attn: Director

Pittsburgh Energy Technology Center
4800 Forbes Avenue
Pittsburgh, PA 15213
Attn: Director

Science Applications, Inc.
Chestnut Ridge Professional Bldg.
Suite 8
Morgantown, WV 26050
Attn: W. G. McGlade
Lu White (6)

US Department of Energy
Nevada Operations Office
P.O. Box 14100
Las Vegas, NV 89114
Attn: Charles Atkinson

US Department of Energy
Laramie Energy Research Center
P.O. Box 3395, University Station
Laramie, WY 82071
Attn: J. Ward Smith

SRI International
333 Ravenswood Avenue
Menlo Park, CA 94025
Attn: D. R. Curran
Stuart L. McHugh
R. L. Burbach

Denver Mining Research Center
US Bureau of Mines
Bldg. 20, Denver Federal Center
Denver, CO 80225
Attn: V. E. Hooker

University of Minnesota
Dept. of Civil and Mineral Eng.
112 Mines and Metallurgy Building
Minneapolis, MN 55455
Attn: Charles Fairhurst

Lawrence Livermore Laboratory
University of California
L-200, P.O. Box 800
Livermore, CA 94550
Attn: M. E. Hanson
Dow Chemical Company
734 Building
Midland, MI 48640
Attn: C. A. Peil

Colony Development Operation
1500 Security Life Building
Denver, CO 80202
Attn: L. L. Ludlam

Science Applications, Inc.
9485 West Colfax Avenue
Lakewood, CO 80215
Attn: Harry E. McCarthy

University of Missouri
104 Rock Mechanics Facility
Rolla, MO 65401
Attn: Ronald Rollins

JAYCOR
1401 Camino Del Mar
Del Mar, CA 92014
Attn: Morris F. Scharff
Maurer Engineering Inc.
10301 NW Freeway, #202
Houston, TX 77018
Attn: A. Richard Sinclair

Sandia Laboratories
Organization 5730
Kirtland Air Force Base
Albuquerque, NM 87115
Attn: H. M. Stoller
Morrison-Knudsen Co., Inc.
400 Broadway
P.O. Box 7808
Boise, ID 83729
Attn: F. Lynn Wilson

Manager, Underground Mining
Science Applications, Inc.
1608 Independence Court
Ft. Collins, CO 80521
Attn: Chapman Young
Schlumberger Well Services
Mechanical Engineering Department
5000 Gulf Freeway
Houston, TX 77023
Attn: Donald J. Garcia

Jet Research Center, Inc.
P.O. Box 246
Arlington, TX 76010
Attn: J. A. Regalbuto
Dresser Industries, Inc.
Dresser Atlas Division
P.O. Box 1407
Houston, TX 77001
Attn: P. A. Pausky

Los Alamos Scientific Laboratory

Los Alamos, NM 87545

W. J. Carter, G-7, MS 329
N. E. Vanderborgh, G-7, MS 329
C. L. Edwards, G-7, MS 329
G. R. B. Elliott, G-7, MS 329
M. A. Fletcher, G-7, MS 329
D. Hopkins, G-7, MS 329
S. C. Schmidt, G-7, MS 329
G. L. Schott, G-7, MS 329
P. E. Trujillo, G-7, MS 329
T. Adams, G-7, MS 329
M. D. Harper, G-7, MS 329
P. Wapner, G-7, MS 329
R. R. Brownlee, G-DO, MS 570
R. J. Hanold, G-DOT, MS 575
W. J. Trela, DIR-O, MS 102
W. E. Deal Jr., M-DO, MS 682
B. G. Craig, M-DO, MS 682
B. G. Killian, J-DOT, MS 668
L. S. Germain, G-DO, MS 570
C. W. Mautz, M-3, MS 960
J. D. Jacobson, M-4, MS 940
J. R. Travis, M-3, MS 960
J. M. Walsh, M-4, MS 940
D. J. Erickson, M-6, MS 970
S. P. Marsh, M-6, MS 970
B. W. Olinger, M-6, MS 970
T. E. Springer, E-4, MS 429
J. N. Johnson, T-14, MS 214
R. D. Baker, CMB-DO, MS 756
R. J. Bard, CMB-8, MS 734
J. P. Bertino, CMB-8, MS 734
J. A. Jackson, Jr., G-7, MS 329